



SPE 140507

Hydraulic Fracturing, Microseismic Magnitudes, and Stress Evolution in the Barnett Shale, Texas, USA

John P. Vermilyen, SPE, and Mark D. Zoback, SPE, Stanford University

Copyright 2011, Society of Petroleum Engineers

This paper was prepared for presentation at the SPE Hydraulic Fracturing Technology Conference and Exhibition held in The Woodlands, Texas, USA, 24–26 January 2011.

This paper was selected for presentation by an SPE program committee following review of information contained in an abstract submitted by the author(s). Contents of the paper have not been reviewed by the Society of Petroleum Engineers and are subject to correction by the author(s). The material does not necessarily reflect any position of the Society of Petroleum Engineers, its officers, or members. Electronic reproduction, distribution, or storage of any part of this paper without the written consent of the Society of Petroleum Engineers is prohibited. Permission to reproduce in print is restricted to an abstract of not more than 300 words; illustrations may not be copied. The abstract must contain conspicuous acknowledgment of SPE copyright.

Abstract

We present new techniques to analyze the effectiveness of hydraulic fracturing for stimulating production in shale gas reservoirs. The case study we have analyzed involves five parallel horizontal wells in the Barnett shale with 51 frac stages. To investigate the numbers, sizes and types of microearthquakes initiated during each frac stage, we created Gutenberg-Richter-type magnitude distribution plots to see if the size of events follows the characteristic scaling relationship found in natural earthquakes. We found that slickwater fracturing does generate a log-linear distribution of microearthquakes, but that it creates proportionally more small events than natural earthquake sources. Finding considerable variability in the generation of microearthquakes, we have used the magnitude analysis as a proxy for the “robustness” of the stimulation of a given stage. We have found that the conventionally fractured well and the two alternately fractured wells (“zipperfracs”) were more effective than the simultaneously fractured wells (“simulfracs”) in generating microearthquakes.

We also found that the later stages of fracturing a given well were more successful in generating microearthquakes than the early stages. This increase in microearthquake activity in the latter frac stages corresponded with an increase in the instantaneous shut-in pressure (ISIP). The net ISIP increase was most pronounced in the simulfrac wells and least pronounced in the zipperfrac wells. We have attempted to model this increase as a cumulative “stress shadow” using an elastic crack-opening model. However, even the maximum reasonable propped fracture aperture causes a stress increase that is less than what was measured in the wells. Since the fracturing of the simulfrac wells took only half the time of the fracturing of the zipperfrac wells, we believe that poroelastic effects associated with time-dependent leak-off is controlling the rate of ISIP escalation and the increase in microseismic creation. We are incorporating poroelasticity in the model to fully integrate stress evolution and permeable volume creation.

Introduction

The ultimate determinant of hydraulic fracturing success is the economic production of natural gas enhanced by the fracturing process. However, production goals may not be reached until weeks, months, or even years after stimulation occurs. Thus, methods to determine the success of fracturing either soon after the operation concludes or even during the hydraulic fracturing job itself are extremely important. Microseismic methods to evaluate stimulation success are most often based on the location mapping of events, despite high location uncertainties and poor detection thresholds. To overcome some of these limitations, we present in this paper new techniques to analyze the effectiveness of hydraulic fracturing success using magnitude relationships that are easily computed from standard microseismic monitoring output. We then place these results in a geomechanical context to better understand the evolution of pore fluid pressure, induced shear fracturing, and stress in the reservoir during slickwater fracturing.

Background

Microseismic monitoring methods were developed to directly observe the fracturing and stimulation process during slickwater hydraulic fracturing. These direct observations address the difficulty (and non-uniqueness) of attempting to interpret fracture creation based solely on the pumping and treatment information. Typical outputs from microseismic monitoring projects are the x-y-z locations, location uncertainties, origin times, and magnitudes of the microseismic events induced during the hydraulic fracturing process. Various techniques have been used to interpret this seismological information into information on the fracture network created during the stimulation process. Warpinski (2009) and Mayerhofer et al. (2010) recently reviewed many of the techniques used to interpret the microseismic data generated during hydraulic fracture monitoring.

The most common application of microseismic monitoring is to simply map the approximate dimensions of the stimulated region and the major fracture pathways through the stimulated volume. However, the routine residual error in the location of a single event is on the order of tens to a hundred or more feet (Maxwell, 2009; Kidney et al., 2010), which in many cases approaches the lateral or vertical dimensions of the reservoir into which the fluid is being injected. The uncertainty in event location, combined with systematic errors from the estimate of the velocity structure, makes precise mapping of the induced fracture network highly uncertain. In particular, attempts to quantify the surface area of the induced fracture network by linking events seemingly related in time and space will likely greatly underestimate the total surface area created in the reservoir. Mapping fracture planes using the focal mechanisms of detected events has been more successful (Williams-Stroud, 2008; Baig and Urbancic, 2010; Eisner et al., 2010) but this technique may unfortunately remain of limited application due to the need for multiple seismometer arrays to generate the focal mechanism solutions.

A better metric for quantitative comparison may be the total volume in which microearthquakes have occurred, a value commonly called the stimulated reservoir volume (SRV). Calculating the SRV usually involves the mapping of bounding volumes around the detected events and then the summation of those volumes to determine the total SRV in a given reservoir. While affected by the uncertainty in microearthquake locations, the measurement of the total stimulated volume eliminates the bias of trying to pick fracture pathways and can allow for comparison between different stimulation projects. Case studies of SRV analysis in Mayerhofer et al. (2010) showed that SRV often correlates well with production data on both a cumulative 6-month and 3-year basis.

Despite this apparently successful correlation, there are still challenges to using SRV as the primary metric for hydraulic fracturing success. Firstly, SRV analysis ignores both the size and the density of the fractures created within the stimulated volume. The size and the density of fractures are likely the key factors controlling access to the low permeability gas shale matrix within the overall stimulated volume. Secondly, SRV analysis in practice often assumes symmetric distribution of events in regions beyond the detection limit of the seismic array, when in fact it is precisely the asymmetric distribution of the fractured volume that we are interested in observing. In addition, when computing the SRV from multi-stage hydraulic fracturing in closely-spaced parallel wells, there is a risk of double-counting total “stimulated volume” if overlapping regions of events from separate wells or stages provide less net enhanced production than identically sized, non-overlapping regions. Lastly, the uncertainty in event locations leads to overestimates of the SRV when using a single string of seismometers. The outermost events by definition provide the boundaries of the stimulated volume, yet they have the largest uncertainties in their location due to their distance from the sensor array. Thus, total measured SRV is dependent on the details of acquisition geometry and processing methods, creating challenges when comparing different stimulation projects on the basis of SRV.

Both SRV analysis and fracture mapping utilize only the locations of the mapped events, ignoring additional information available in the seismic signal. Urbancic and Maxwell (2002) looked at the apparent stress drop of events to differentiate between shear and non-shear components of deformation, which they suggest could allow for mapping of the most permeable pathways in the reservoir. Trying to incorporate fracture density into SRV analysis, Maxwell et al. (2006) combined total seismic moment with SRV to generate a combined stimulation metric in a Barnett shale well. This combined metric was found to correlate well with production in cases where production did not correlate well with SRV alone. They also mapped the moment density of events from the stimulation to try to image the regions where the largest deformation has occurred. Due to the $\sim 32\times$ difference in moment between events just one magnitude value apart (Hanks and Kanamori, 1979), the total measured moment as well as the moment density maps were dominated by the few largest events. Thus, it may be difficult to extend their analysis due to the dependence of total moment on the random occurrence of the few largest events. Maxwell et al. (2008) looked at the rate of moment generated during hydraulic fracturing. This rate analysis is useful in seeing if a fracturing job has stalled in generating new fractures, allowing for on-the-fly changes in the stimulation method. However, they found that total moment correlates poorly with total injection volume, again likely due to the few largest events dominating the total moment.

Microearthquake Magnitude Scaling

Urbancic et al. (1999) suggested using the relative frequencies of microearthquake event magnitudes to determine the evolution and behavior of hydraulic fracturing. This method can provide an estimate of fracturing activity level that is independent of both sensor bias and the random occurrence of the largest few events. We have expanded upon the technique introduced by Urbancic et al. (1999) and apply it to a case study in the Barnett shale. Before detailing the methodology we have used, we will first discuss the theory and evidence for consistent earthquake magnitude scaling relationships and how it has previously been applied to microearthquake data and fracture generation in a reservoir.

Gutenberg and Richter (1944) provided evidence for a consistent scaling relationship in earthquake magnitudes. In their compilation of earthquake data from California and the world, they found that the total number of earthquakes at a given magnitude obeyed a log-linear relationship, with the logarithm of total earthquakes at a given magnitude decreasing with a slope of about 1 for each increase in magnitude unit. This slope has become known as the b-value, and has been found to be ~ 1.0 for nearly all crustal volumes containing naturally-occurring earthquakes. The consistency of this earthquake scaling relationship has been extensively studied over the past six decades, both as an important parameter in estimating earthquake recurrence and as an insight into the fundamental processes of earthquake generation and fault evolution.

While the consistent slope of the magnitude-frequency relationship for relatively large earthquakes has been well established, the extension of this relation down to smaller events has been subject to considerable debate. Aki (1987) found

that the magnitude-frequency relation for events of $M < 3$ was not followed, leading to far fewer small events than would be predicted if self-similarity continued. Trifu et al. (1993) found departures from a constant b-value of about 1 for events between $M -0.5$ and $M 0$ in a dataset recorded in a mine. In contrast, several authors have found b-values of about 1 for events down to $M -1$, and even down to $M -3$, in careful studies from seismic networks installed in mines, boreholes, and at the surface (Sprenke et al., 1991; Abercrombie, 1996; von Seggern et al., 2003; Oye et al., 2005; Boettcher et al., 2009).

Despite the ongoing debate over the causes (and the consistency) of the earthquake magnitude-frequency relationship for extremely small events, the microearthquakes generated by hydraulic fracturing can still be investigated using similar methodologies as the studies cited above. Urbancic et al. (1999) analyzed the magnitude-frequency relationship from a single-well, multi-stage hydraulic fracturing microseismic dataset. They found that the scaling of events was approximately log-linear within the range of event magnitudes that were fully detected by the seismic array. They then calculated both the b-value and the “activity level” of the generated events across space and time in the reservoir. The b-value was used to investigate the ratio of large and small events and the failure mechanisms that generated those events. The activity level was then used to quantify the rate of seismicity and thus the density of fractures created in the reservoir.

We have developed a frequency-magnitude analysis methodology that is similar to Urbancic et al. (1999), but more appropriate for comparison of the individual stages and individual wells of complex hydraulic fracturing experiments. We present our methodology in detail below and then apply it to a case study in the Barnett shale.

Methodology

As discussed above, we use microseismic magnitude scaling to create a stimulation success metric that can compare the success of different fracture operations yet is fully independent of the seismic acquisition geometry. This technique is based on fitting a log-linear scaling relationship, $\log_{10}(N \geq M) = a - bM$, to the microseismic magnitude data. Fitting the event magnitudes to this equation determines the b-value, which is the slope of the log-linear curve, and the a-value, which is the log of the total number of events $\geq M = 0$. For areas with identical b-value scaling parameters, this intercept is a robust measure of the relative activity level for the two areas. For example, when fitting a decade’s worth of seismicity from New England and a decade’s worth of seismicity from a New England-sized portion of California, the two curves will likely have a very similar b-value. However, the California curve will have a much greater a-value than the New England curve. The a-value, therefore, is an indication of the relative seismicity levels in these two areas.

This principle also allows us to analyze differences in activity level for microseismicity found in a reservoir, acknowledging the fact that the detection of the very smallest events will be affected by the distance between the events and the monitoring arrays. For example, Figure 1 schematically demonstrates what the magnitude scaling curves might look like for a hydraulic fracturing stage measured by two different seismic arrays, one close to the fractures and one farther away. The closer array detects many more total events, but the scaling curves are identical above the magnitude threshold of the more distant array. Thus, fitting the equation above to only the log-linear portion of the scaling curve can isolate sensor effects quite easily. In the case of multiple hydraulic fracturing stages, it is thus possible to determine the robustness of fracture creation independent of array location. For example, Figure 2 shows two fracture stages detected by a single seismic array. More total events are detected for the stage closest to the array. However, the farther stage was in fact more robust overall, and this difference in activity level is picked up by fitting the log-linear portions of the magnitude scaling curve.

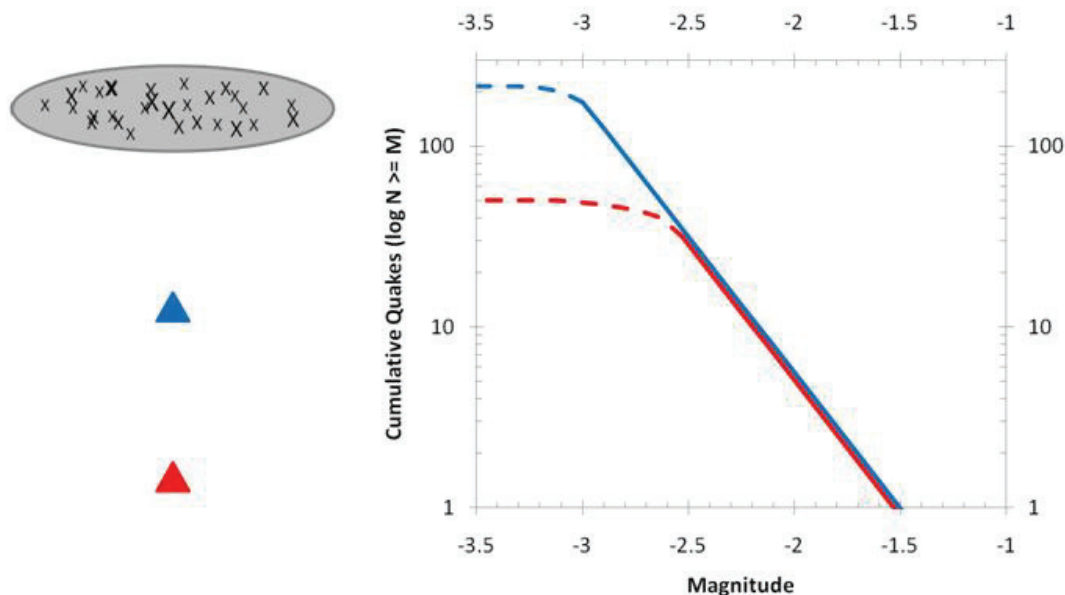


Figure 1: Schematic magnitude scaling curves for a hydraulic fracturing stage as measured by two different seismic arrays, one close to the fractures (blue) and one farther away (red).

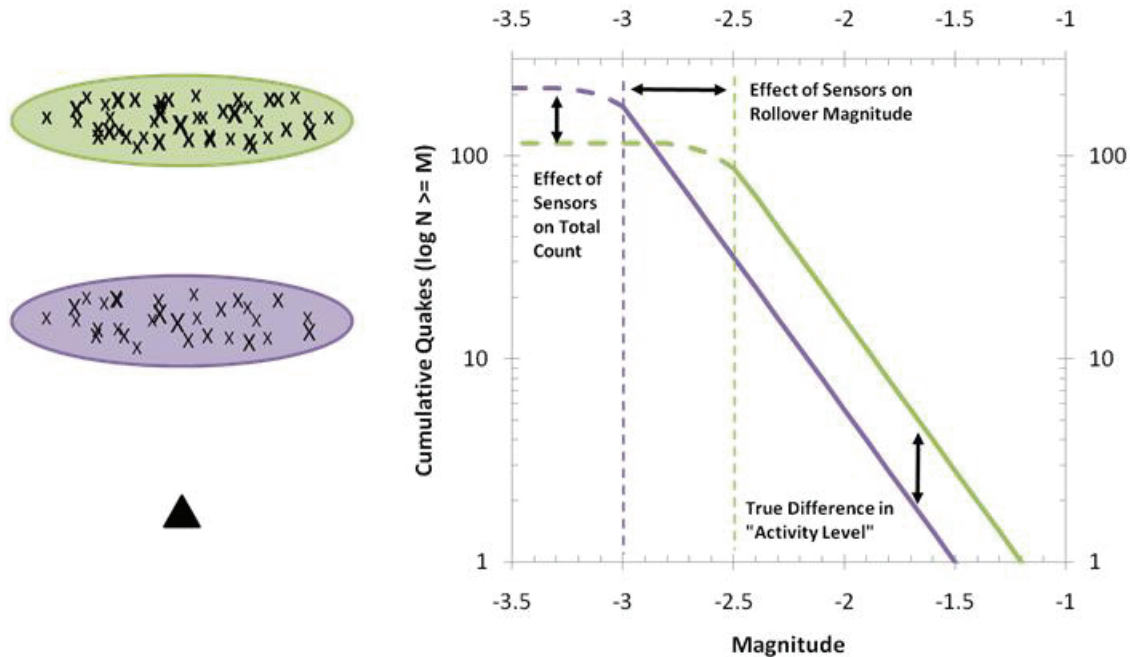


Figure 2: Magnitude scaling curves for two fracture stages detected by a single seismic array. More total events are detected for the stage closest to the array (purple), but the stage further away (green) is in fact more robust.

Quantifying Microseismic “Activity Level”

The b-value can provide important information on the distribution of triggered events as well as insight into the mechanisms of fracture creation in the reservoir. However, the a-value is in fact a more direct measure of the success of hydraulic fracturing since it is equal to the actual number of earthquakes predicted to be $\geq M = 0$. For two populations with the same b-value, the traditional a-value uniquely describes the difference in activity between the populations at all magnitudes. However, for populations with different b-values, the actual quantity of events within the magnitude range of interest could differ much more than is expected from a small difference in a-values. Thus, the typical a-value from Gutenberg-Richter type analysis can't be used as a comparative metric for populations with varying b-values.

To better measure the activity level for hydraulic fracturing, we calculate the cumulative number of events greater than or equal to the magnitude that is the detection threshold for the stage with the worst detection sensitivity. This metric is similar to Urbancic et al. (1999), but uses a detection threshold that ensures that each stage can be quantitatively compared.

Study Area

The schematic geology of the study area can be seen in Figure 3. In this part of the Ft. Worth Basin, the Barnett lies directly on the Ellenberger limestone, a water producing interval that will lead to an unsuccessful well if intersected by the stimulated fractures. Thus, the horizontal wells in the study area were drilled in the upper Barnett in an attempt to avoid the Ellenberger, despite the lower Barnett being considered the core producing zone of the field. While no core samples were available for this field area, inspection of the FMI log reveals mostly thin, healed natural fractures, filled with calcite.

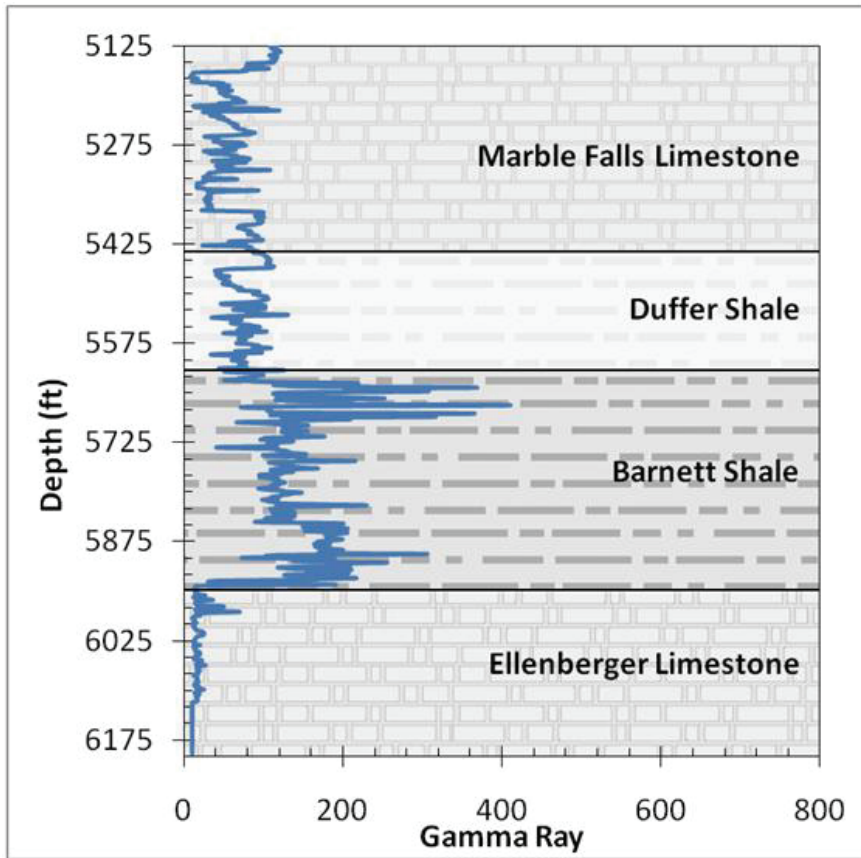


Figure 3: Well C Vertical Pilot gamma ray and interpreted geologic formations in study area.

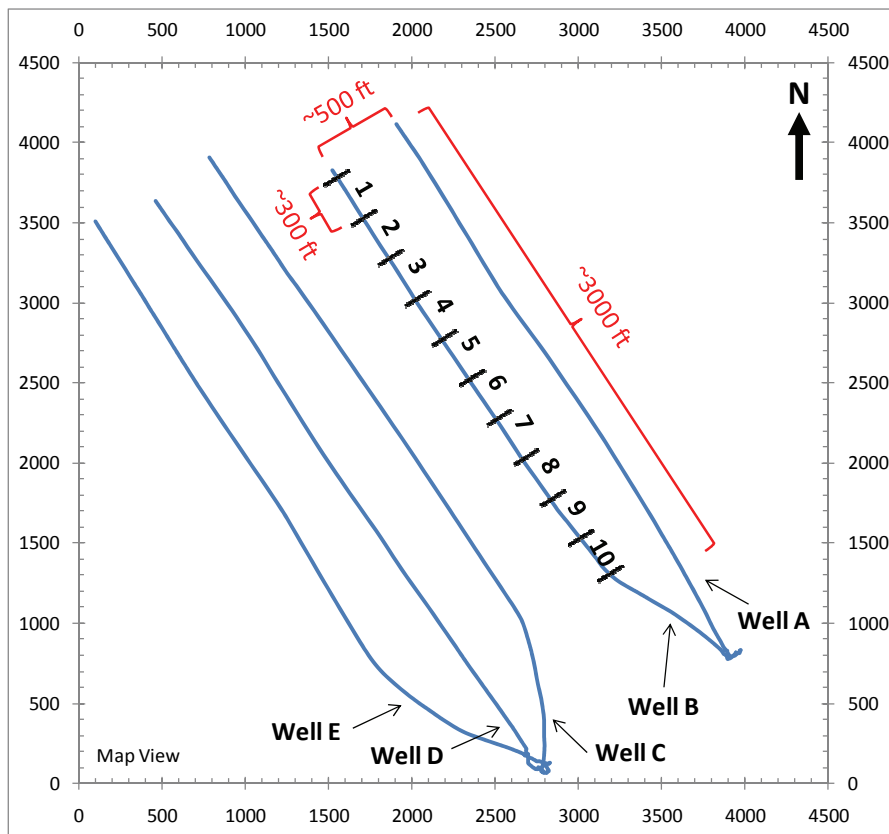


Figure 4: Study area of five parallel horizontal wells, referred to as Wells A-E. Each well was fractured in ~10, 300-foot long stages.

Drilling and Logging Program

The study area consists of five parallel, horizontal wells, as seen in Figure 4, here referred to as Wells A-E. Well C was first drilled vertically through the Barnett as a pilot well, and then comprehensively logged, including FMI and dipole sonic logs. The horizontal section of Well C was logged for FMI. All other wells were logged only with gamma ray during drilling.

Hydraulic Fracturing Program

All of the wells were cased, cemented, and then perforated at 50 ft intervals before being fractured. Wells A, B, D, and E were fractured in 10 stages, while well C was fractured in 11 stages. The stages were approximately 300 feet long, with six perforation clusters spaced equally within each stage. For a typical stage, water and sand were pumped at a rate of 50-60 bpm for ~150 minutes, with pumped water totaling ~325,000 gallons and sand totaling ~400,000 pounds per stage. A few stages received significantly less water and sand than the average stage. In the microseismic analysis presented below, these stages were either removed from the results or noted as atypical.

The five wells were fractured using three different completion procedures (illustrated schematically in Figure 5) in order to test the effectiveness of different fracturing methods. Wells A and B were the first of the wells to be fractured, and were stimulated using a “simulfrac” method. In the simulfrac method, Stage 1 of Well A and Stage 1 of Well B were fractured simultaneously, with the hope that total connectivity between the two wells and the overall stimulated reservoir volume would be greater. The simulfrac proceeded with simultaneous fracturing of stages 2 through 10 moving from the toe to the heel of the wells. During the simulfrac operation, injection into each well was carried out at a rate of 50-60 bpm. Wells D and E were the next group to be fractured, and were stimulated using a “zipperfrac” method. In the zipperfrac method, the fracturing of Stage 1 of Well D was followed by Stage 1 of Well E, which was followed by Stage 2 of Well D, and so on alternating until all stages were completed. Well C was fractured by itself, the last of the five wells to be stimulated. Well C was surrounded by wells that had already been drilled and fractured, thus representing the common case of a well drilled in an infill fashion between existing wells.

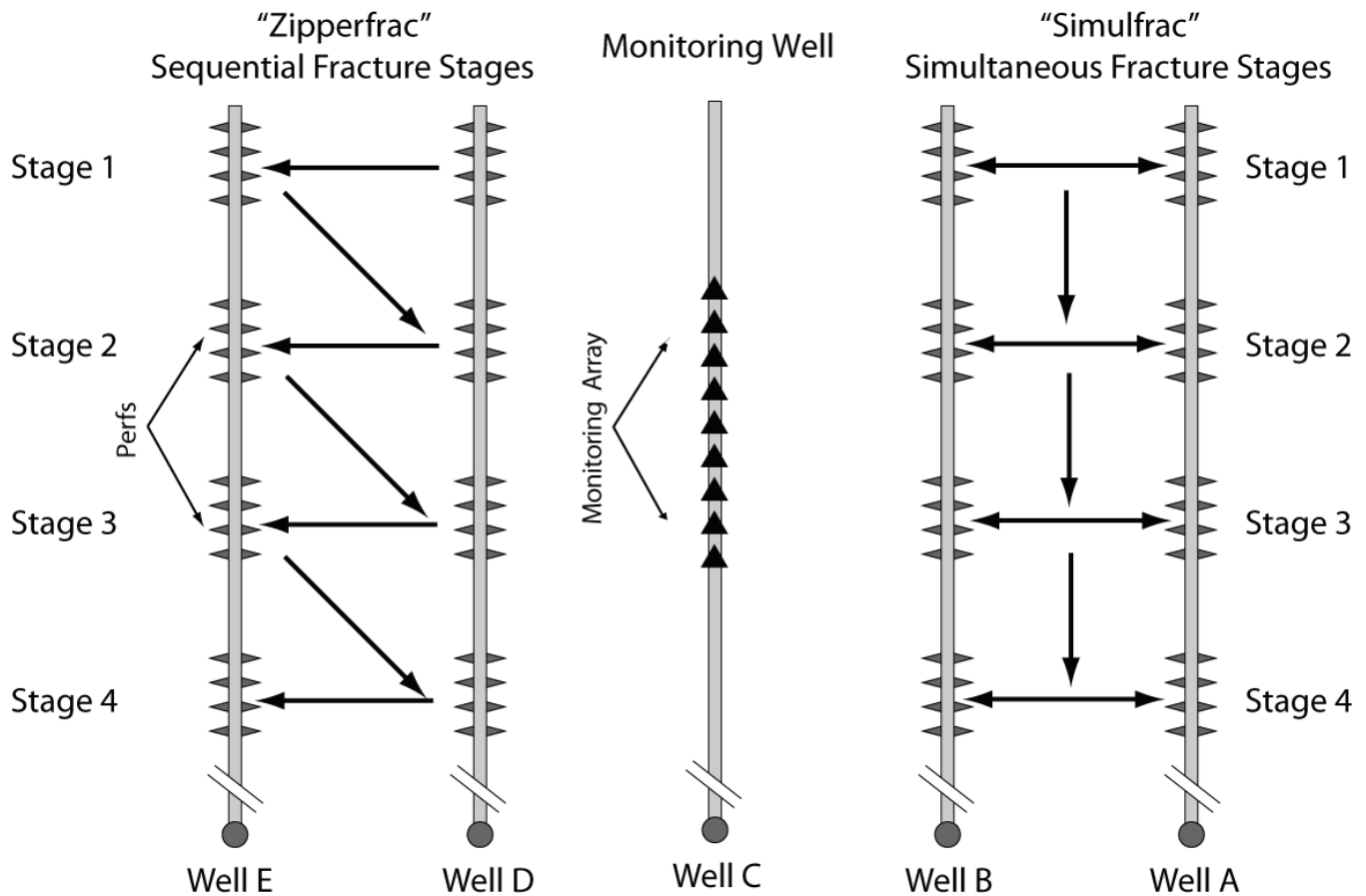


Figure 5: Schematic view of stimulation procedures. Wells A and B were stimulated simultaneously (“simulfrac”). Wells D and E were stimulated sequentially (“zipperfrac”). The monitoring array was moved throughout the operations in order to reduce the distance between the array and the microseismic events.

Microseismic Monitoring Program

All the stages were monitored seismically during fracturing in order to identify microearthquakes. For stimulation of Wells A & B, an array of nine 3-component seismometers spaced 50 feet apart was placed at various positions in Well C. For stimulation of Wells D & E, an array of ten 3-component seismometers spaced 40 feet apart was placed at various positions in Well C. For stimulation of Well C, an array of twelve 3-component seismometers spaced 35 feet apart was placed in the vertical section of Well B. Velocity models were created using well logs and the perf shots. In total, 4,485 events were located from the five stimulated wells by the microseismic contractor (Figure 6).

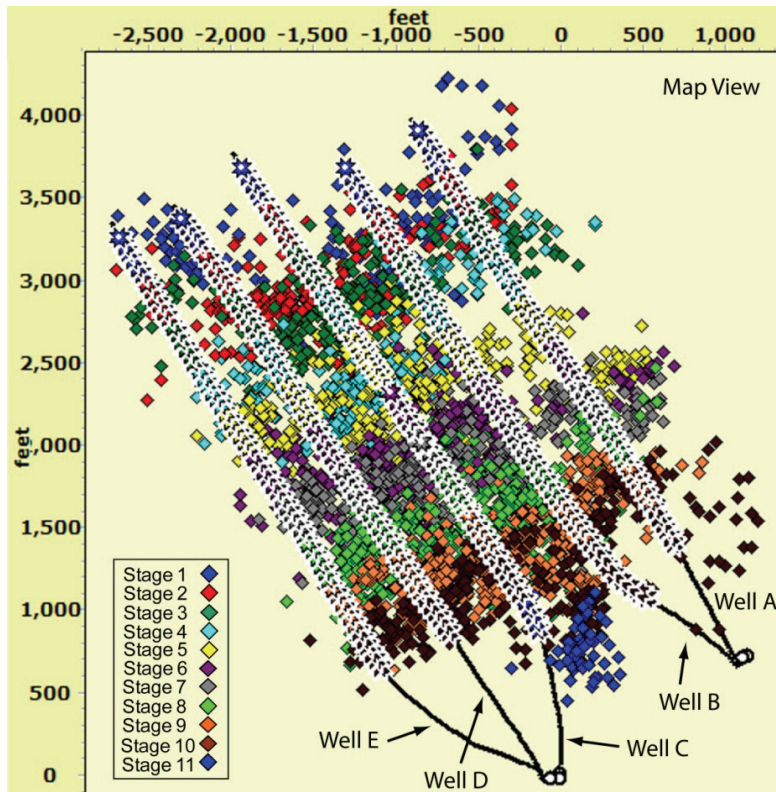


Figure 6: Combined microseismic monitoring results for Wells A-E.

Microseismic Magnitudes

The magnitudes of the microseismic events were calculated by the microseismic contractor. Moment magnitudes were calculated from shear wave amplitudes using a modified Hanks/Kanamori equation (Hanks and Kanamori, 1979). The shear wave amplitudes were corrected for distance and attenuation effects before being used to calculate the seismic moment and the moment magnitude.

We have not attempted to re-calculate the microseismic magnitudes reported by the microseismic contractor. Thus, the accuracy of the individual event magnitudes is dependent on the original methods used by the contractor. A recent paper by Shemeta and Anderson (2010) on calculating magnitudes for microseismic datasets demonstrates the uncertainties introduced by the different techniques used to analyze this type of data. While the moments and magnitudes we have used in this analysis were calculated using shear wave amplitudes, the contractor on this project has also calculated magnitudes using shear wave corner frequencies and found that the calculated event magnitudes had only insignificant differences. Thus, we remain confident that the magnitudes used in this study are as representative of the “true” event magnitudes as is routinely possible to determine given the uncertainty in calculating either shear wave amplitude or corner frequency on such small events.

Results

We calculated the Gutenberg-Richter parameters for all the stages of Wells A-E using least-squares fitting techniques. Two example curves can be seen for Well C Stage 6 and Well C Stage 8 in Figure 7. These two stages exhibit good linear fits with slopes of $b = 1.88$ and $b = 1.51$, respectively. It was found for all the analyzed stages that the b -value was significantly greater than 1, indicating an abundance of relatively small events. Thus, the microearthquakes induced during stimulation in our study area do not follow the same magnitude scaling relation as natural earthquakes.

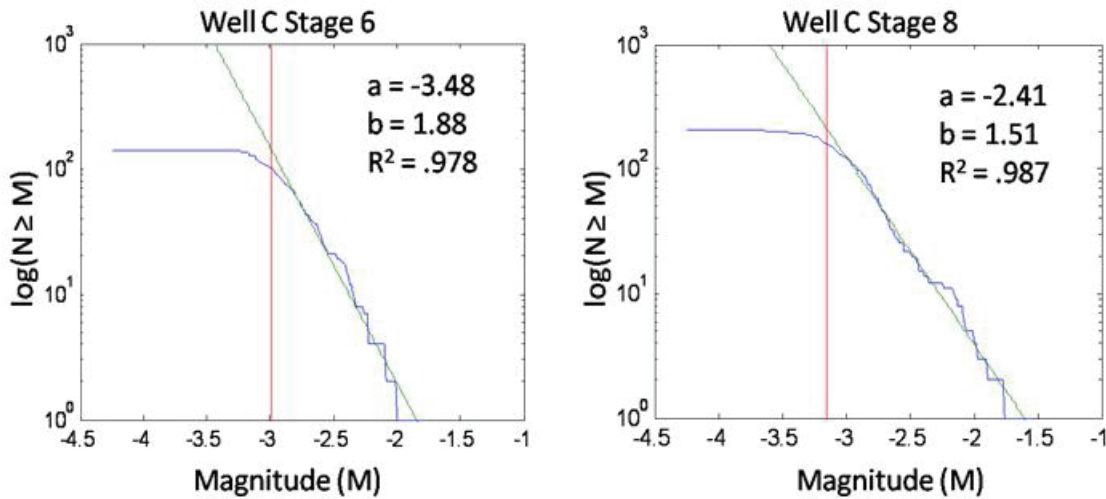


Figure 7: Example cumulative Gutenberg-Richter fits from Well C demonstrating steep, varying b-values that prevent direct comparison of a-value as “activity level” proxy. Note that Stage 8 has a slightly higher detection capability (M -3.2) compared to Stage 6 (M -3.0). Stage 8 is approximately 600 ft closer to the monitoring array.

As seen in Figure 8, there is a large variability in earthquake generation between stages that demonstrates a clear difference in activity level, and thus in the relative success of the stimulation process during hydraulic fracturing. However, the stages of Wells A-E also have a large variation in b-value, thus necessitating an empirical activity level metric as discussed above. In this case, we calculated the total number of events for each stage with magnitude greater than or equal to -2.5. For nearly all the stages, M = -2.5 was within the magnitude region with complete expected detection of events. This metric clearly tracks the variability seen visually between the stages, as demonstrated in Figure 8.

Looking at the per stage average for our metric (Figure 9), it is clear that the simulfracs (Wells A & B) underperform both the zipperfrac (Wells D & E) and the conventional frac (Well C). These results are consistent with conclusions from a stimulated reservoir volume analysis conducted by the microseismic contractor. However, the large variation in stimulation level for the individual stages indicates that there is important variability on a stage-by-stage basis.

To investigate this variability, we have compared the activity level of the individual stages with various reservoir and operational parameters (Figure 10). Gamma ray (and thus clay content/TOC) does not seem to show a strong correlation with activity level, nor does total water or sand injected. However, as seen in Figure 11, the correlation with stage number does indicate that fracturing success increases in the later stages, which will be analyzed further below.

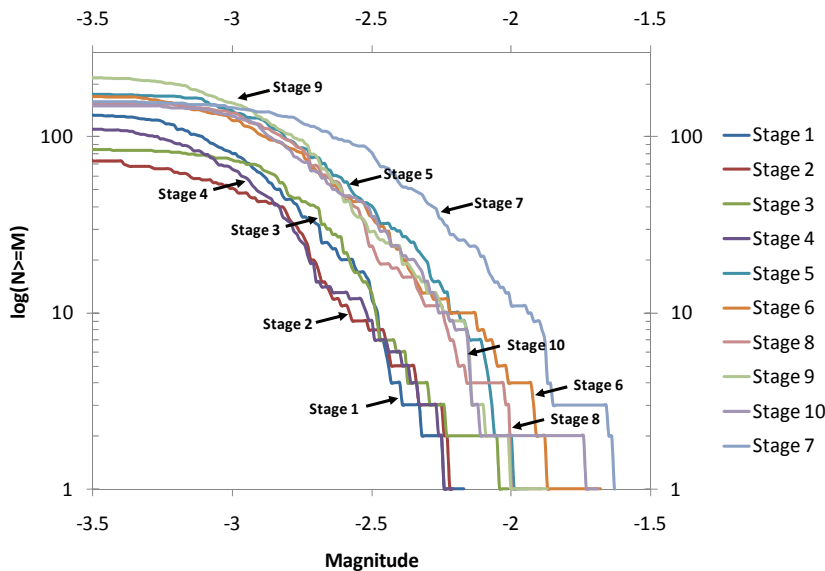


Figure 8: Cumulative Gutenberg-Richter plots from the Well A-B “simulfrac” demonstrating significant variability in earthquake activity between the stages.

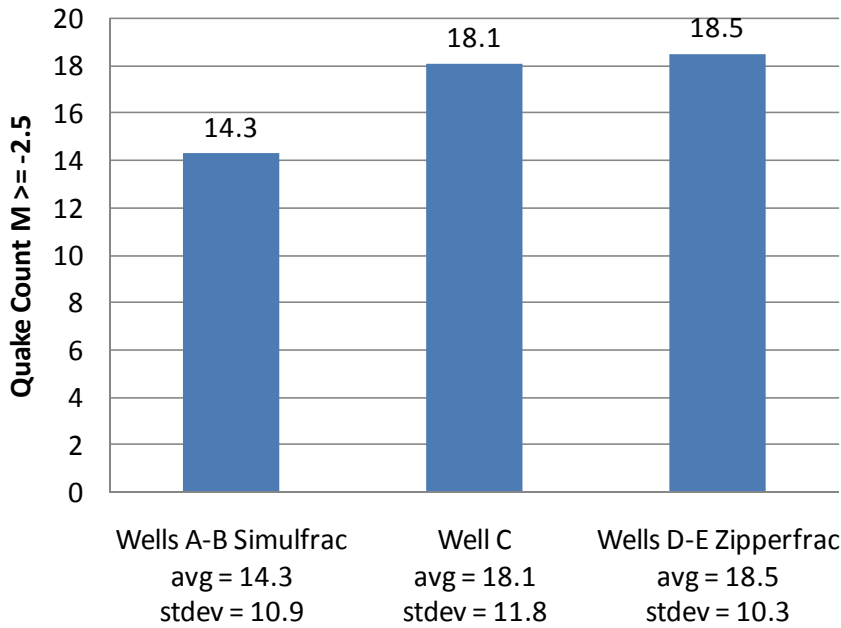


Figure 9: Per stage average quake count for events $M \geq -2.5$ indicates a small advantage for the zipperfrac technique.

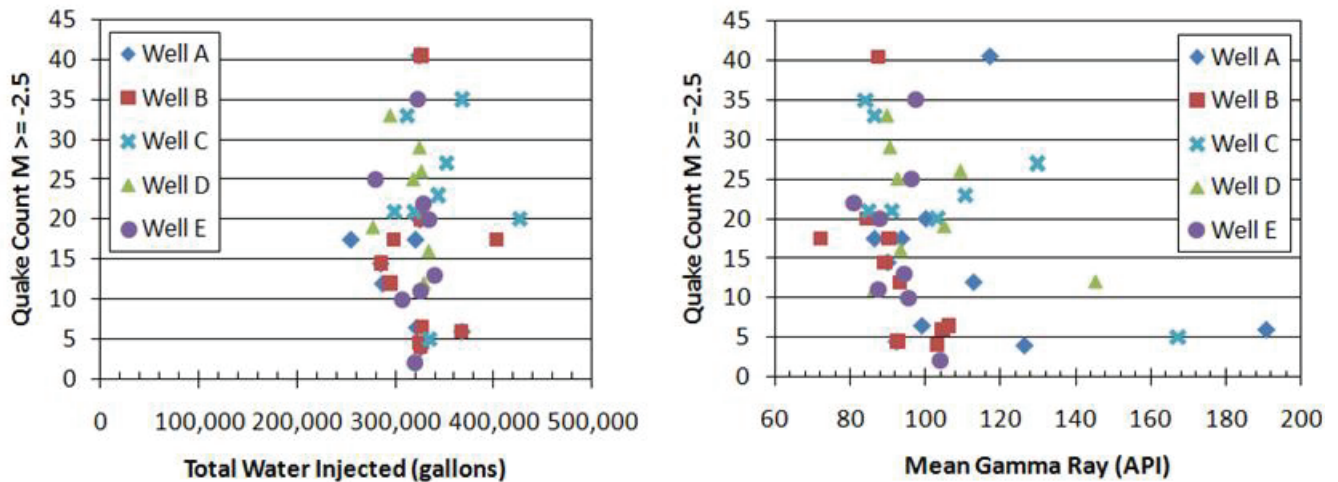


Figure 10: Quake count ($M \geq -2.5$) for all wells shows little correlation with gamma ray or total injected water.

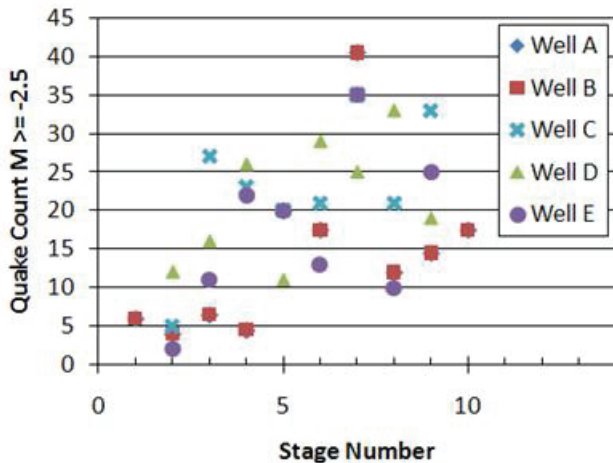


Figure 11: Quake count ($M \geq -2.5$) does show some correlation with stage number.

Measuring and Modeling Stress Evolution During Fracturing

A major goal of our work on the Barnett shale is to better understand fracturing and fluid flow in the reservoir before, during, and after stimulation, with a specific focus on how the stress evolution within the reservoir affects these parameters. To integrate microseismicity, geomechanics, and flow analysis, as well as results from the laboratory studies on the Barnett and other gas shales, we are looking at various ways to model stress, fracturing, and fluid flow.

Base Geomechanical Model

As a first step in our analysis, we created a geomechanical model of the field area. This model is used as the base model to understand the evolution of stress in the reservoir after hydraulic fracturing begins.

We have followed the methodology for determining the in situ stress state from Zoback et al. (2003):

1. Calculate elastic moduli from velocity, density logs, and laboratory data;
2. Calculate the vertical stress (S_v) by integrating the density log;
3. Identify the occurrence of drilling induced tensile fractures and wellbore breakouts using electrical image log and caliper data to determine stress orientation;
4. Utilize uniaxial compressive strength (C_o) from lab data to analyze compressive wellbore failures;
5. Interpret minifrac and leak-off tests to determine the allowable range of S_{hmin} magnitudes and pore pressure (P_p);
6. Interpret available data to constrain the possible values of S_{Hmax} .

We found S_v to be slightly elevated above expected values at 1.1 psi/ft. We estimated S_{hmin} from the instantaneous shut-in pressure (ISIP) measured at the toe of Well C and confirmed by the ISIP from other stages. S_{hmin} is estimated to be between 0.63 to 0.67 psi/ft. The vertical pilot section of Well C contains a few inclined, curved tensile features, indicating that the stress tensor may be slightly tilted with respect to the vertical well axis. Modeling of these inclined tensile features is ongoing, and for this analysis they are treated as standard drilling induced tensile fractures. The horizontal section of Well C contains distinct stress zones demonstrating mixtures of axial, transverse, and curved tensile features. Stress modeling of the tensile features seen in the horizontal section of Well C demonstrates that the stress state is normal faulting, with an S_{Hmax} below 0.8 psi/ft. The normal faulting stress environment with relatively low horizontal stress anisotropy is fairly typical for the Barnett shale.

ISIP Escalation

We found during our initial geomechanical modeling that the instantaneous shut-in pressure (ISIP) values for each well changes as the fracturing sequence progresses. The ISIP is determined after pumping is shut off at the point when the main fracture closes instantaneously and the slope of the pressure decline curve changes. In cases where pumping rates and total pumping duration are low, ISIP can give a very accurate determination of the least principal stress magnitude. However, for a typical Barnett stage with over two hours of pumping at a high rate, the ISIP is at best an approximation of the least principal stress magnitude.

Schematic and actual examples of ISIP are seen in Figure 12. For Wells A-E, because the fracturing fluid was of such low viscosity, the pressure declines very quickly. There was also a large water hammer effect, leading to poor accuracy of measured ISIP to no better than ± 50 psi.

Calculated ISIP values for all wells, all stages are seen in Figure 13. For all the wells, the ISIP values increase moving from the toe to the heel in a steady progression, except that there is a fall-off for the last few stages in Wells A, B, and C. A similar effect has been reported in the gas shale literature and explained as a “stress shadow” related to sequential propped planar fractures (East et al., 2004; Fisher et al., 2004; Soliman et al., 2008; Waters et al., 2009).

Interestingly, the simulfrac wells (A and B) exhibit the greatest increase in ISIP, while the zipperfrac wells (D and E) exhibit the least. The ISIP for wells A and B increases by over 1200 psi, while it increases by less than 600 psi for wells D and E, with well C in the middle. As seen in Figure 14, there seems to be a correlation between microseismic activity level and the ISIP value for an individual stage. However, this correlation follows a different trend for the simulfrac wells and the zipperfrac wells. The simulfrac wells escalate to a higher ISIP by the end than the zipperfrac, but actually show less total seismic activity. Thus, while an increase in the minimum principal stress is correlated with additional microearthquake production, the exact impact of these stress changes on the reservoir seems to be controlled by the method of fracturing.

Modeling the Changes in ISIP

To better understand why the ISIP increases with later stages, we have utilized a relatively simple analytical model of the “stress shadow” effect of closely-spaced propped fractures on the magnitude of the minimum horizontal stress. The ten stages of an individual well create at a minimum ten large, planar fractures spaced on average 300 feet apart. These main fractures, which are orthogonal to the direction of S_{hmin} , are likely to cumulatively interact with each other to increase the minimum horizontal stress magnitude in the reservoir, and thus the measured ISIP. This cumulative increase may be transient when the main fractures are held open by the pumping pressure, but they are also likely semi-permanent due to the emplaced proppant keeping the main fracture plane open. Thus, they may impact the stress felt by the next hydraulic fracture even if the pressure in the previous fracture has declined.

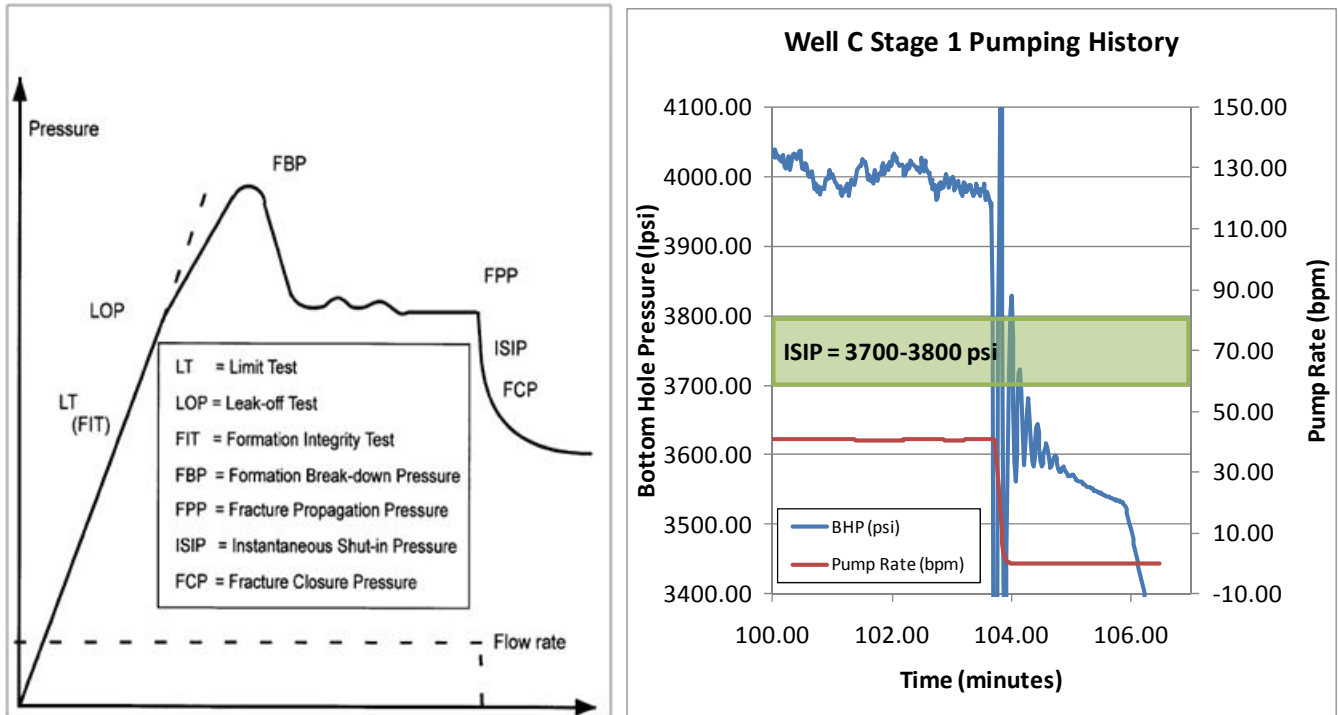


Figure 12: (left) Example extended leak-off test demonstrating multiple ways to directly measure S_{hmin} , including the Instantaneous Shut-In Pressure (ISIP). After Gaerenstroem et al. (1993). (right) Example ISIP curve from Well C Stage 1. Water hammer effect causes ISIP precision to be $\pm \sim 50$ psi.

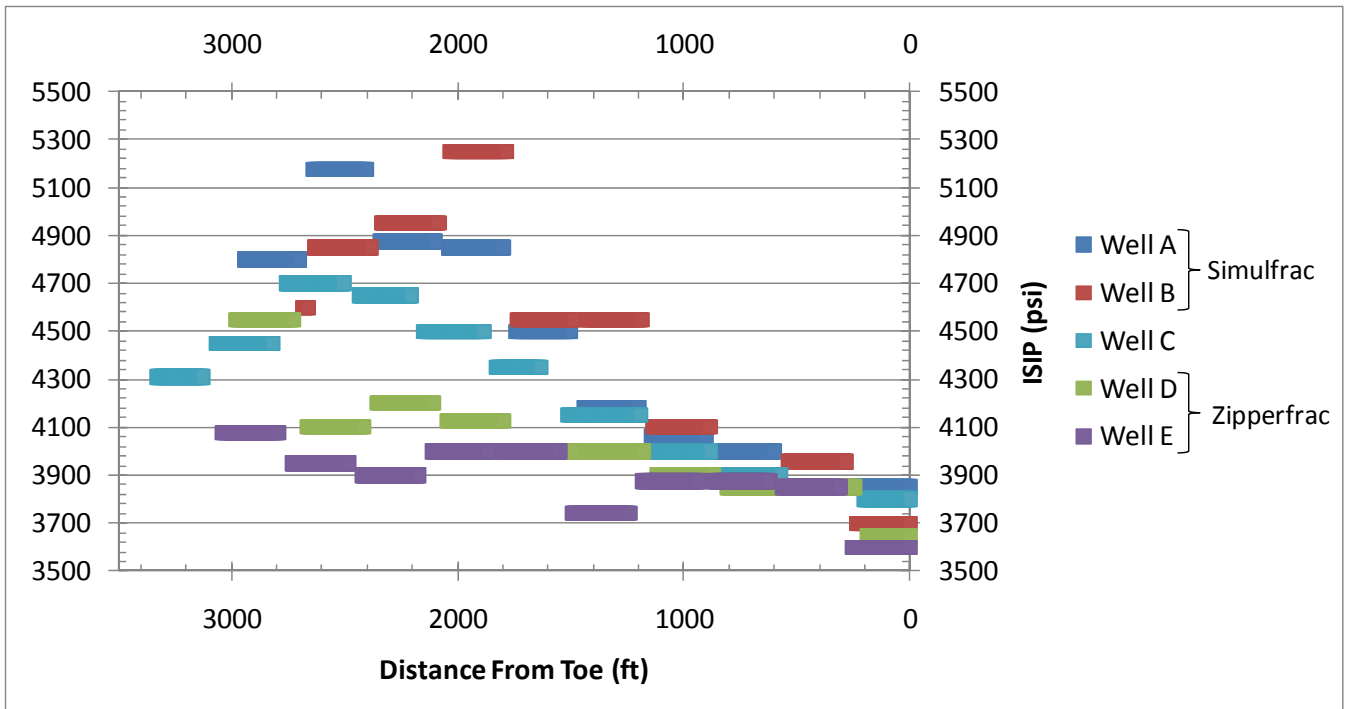


Figure 13: ISIPs escalate from toe to heel in all wells. The simulfrac wells, A & B, escalate the most, while the zipperfrac wells, D&E, escalate the least.

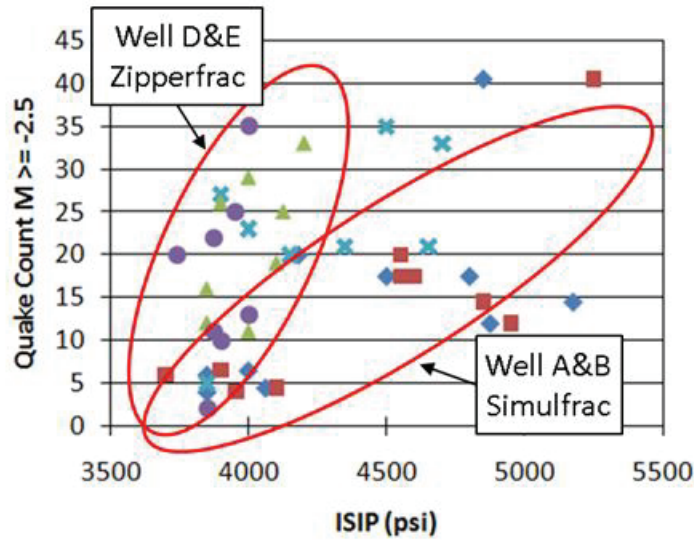


Figure 14: The correlation between ISIP and quake count follows a different trend for the simulfrac wells and the zipperfrac wells.

To model these planar fractures, we have first used a very simple planar crack model from Sneddon (1946). The fractures are 2-dimensional and are modeled as infinite in the S_{Hmax} direction (which is a reasonable approximation since fracture length for our wells is greater than three times the fracture height). The equations used to model the fractures are as follows:

$$\begin{aligned} \sigma_A &= -P \left\{ \frac{L}{\sqrt{L_1 L_2}} \cos \left[\theta - \frac{1}{2} (\theta_1 + \theta_2) \right] - 1 \right\} \\ \sigma_B &= P \left\{ \frac{L \sin \theta}{h/2} \left(\frac{h^2/4}{L_1 L_2} \right)^{3/2} \sin \left[\frac{3}{2} (\theta_1 + \theta_2) \right] \right\} \\ \tau_{xy} &= -P \left\{ \frac{L \sin \theta}{h/2} \left(\frac{h^2/4}{L_1 L_2} \right)^{3/2} \cos \left[\frac{3}{2} (\theta_1 + \theta_2) \right] \right\} \\ \sigma_y &= 2\mu\sigma_A \\ \sigma_z &= \sigma_A + \sigma_B \\ \sigma_x &= \sigma_A - \sigma_B \end{aligned}$$

$$\begin{aligned} L &= \sqrt{x^2 + z^2} \\ \theta &= \tan^{-1} \left(\frac{x}{-z} \right) \\ L_1 &= \sqrt{x^2 + (z + h/2)^2} \\ \theta_1 &= \tan^{-1} \left(\frac{x}{-z - h/2} \right) \\ L_2 &= \sqrt{x^2 + (z - h/2)^2} \\ \theta_2 &= \tan^{-1} \left(\frac{x}{h/2 - z} \right) \end{aligned}$$

where σ_x is the S_{hmin} magnitude, σ_y is the S_{Hmax} magnitude, σ_z is the S_V magnitude, P is the effective “pressure” keeping the fracture open, h is the fracture height, z is the distance above or below the centerline of the fracture, and x is the distance away from the fracture plane, following the nomenclature of Warpinski and Branagan (1989).

For our model, fracture height and spacing were both set at 300 feet, which is representative of the distances seen in the microseismic monitoring. Opening pressure was set at 750 psi, which is equivalent to an approximately 2 cm crack for elastic moduli appropriate to the reservoir.

Results from a single crack, as well as a series of sequential cracks, are seen in Figure 15 below. The stress increase from a single crack decays quite quickly away from the fracture plane, thus leading to modest cumulative stress increase compared to the amount of stress increase seen very close to the fracture plane. In all, the cumulative stress increase is less than 400 psi, well below the increase in ISIP seen in wells A, B, and C. Since the model already assumes a relatively large 2 cm crack opening, it does not seem that the actual ISIP increase can be fully modeled using just cumulative planar fractures. Moreover, there is no obvious mechanism to explain why the stress in the zipperfracs and simulfracs would differ so much if changes were only coming from sequential propped planar fractures.

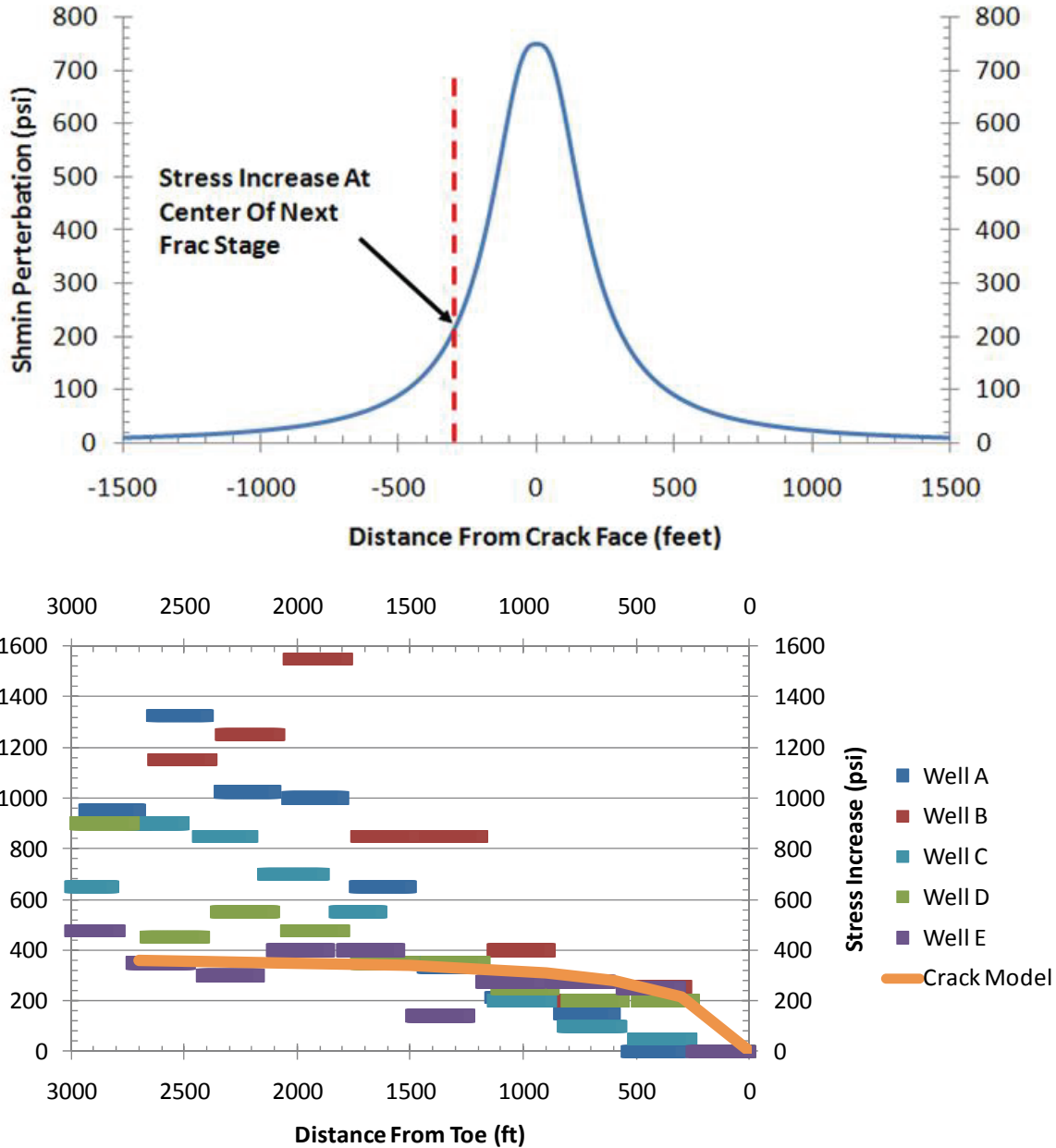


Figure 15: (top) Stress increase from a single semi-infinite Sneddon-type crack 300 ft high. Fluid pressure opening crack in model is 750 psi, equivalent to ~2 cm of total opening. (bottom) Results of modeling multiple sequential cracks, showing progressive escalation in stress, but not as large as seen in Wells A, B, and C.

Modeling Poroelastic Effects

Given that purely planar fractures can't explain the increase in ISIP in Wells A-E, it is possible that a poroelastic effect from the large amounts of pumped water during the successive stages are controlling the stress change in the reservoir. One piece of evidence in favor of a poroelastic effect is that the simulfrac wells were fractured in half the total time that the zipperfrac wells were. With only half the time for pressure to leak off, the measured ISIPs in the simulfrac wells are much greater than those seen in the zipperfrac wells. Although there is a lot of scatter, Figure 16 shows that microseismic creation seems to best correlate with total elapsed time from the beginning of a given well's first stage, suggesting that greater leak off into the reservoir stimulates a greater number of microearthquakes.

Modeling to better understand this poroelastic impact has just begun. We are using a coupled geomechanics and flow simulator to better understand the evolution of pore pressure and stress throughout the fracturing process. By fitting both the generated clouds of seismicity and the increase in ISIP, we should gain new insight into how the fracture network and stress grow during the stimulation process, and thus have new insight on the creation of the permeable fracture network that controls fluid flow in the Barnett shale.

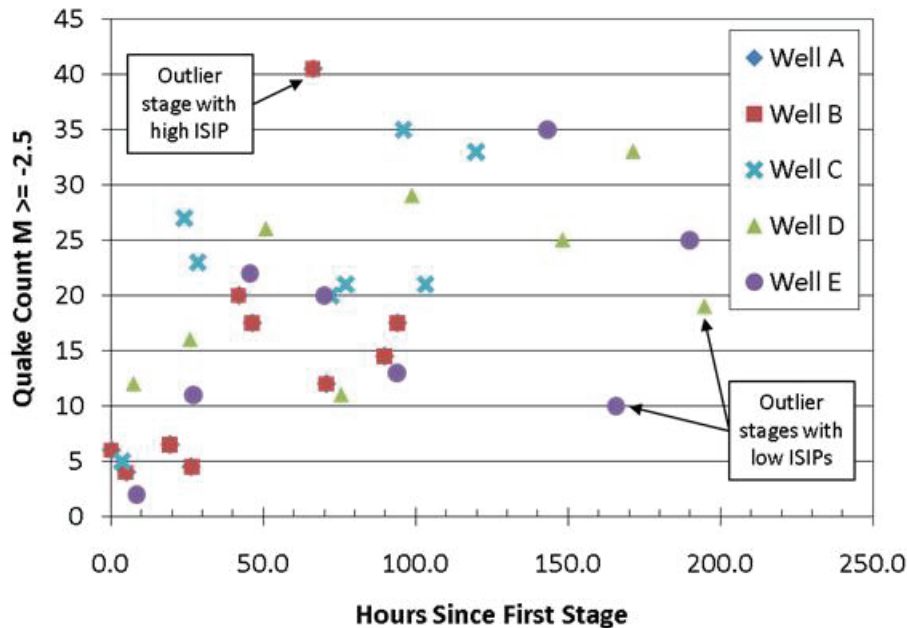


Figure 16: Earthquake creation seems to best correlate with total elapsed time from the beginning of a well's first stage, suggesting that cumulative leak off helps stimulate microearthquakes.

Conclusions

We have used techniques from earthquake seismology to compare the “activity level” of a fracture stage, suggesting a new way to measure stimulation success that does not involve subjective mapping of fractured volumes. When using this magnitude-based metric, we have found significant differences in stimulation robustness for the different fracturing procedures seen in our study area. There is a complicated interdependence of stress, pressure, and stimulation in the study area, and our initial attempts to model these changes analytically have not been able to explain all the observed results.

Future work will involve refining our geomechanical understanding of the study area and attempting to model the evolution of stress and the creation of a permeable fracture network through the use of coupled flow and geomechanics simulators. The conclusion of this work should give a new insight into the lifecycle of a Barnett shale reservoir as well as suggest new techniques for modeling and analyzing the data collected during a gas shale hydraulic fracture operation.

Acknowledgments

We would like to thank ConocoPhillips for providing the data used in this study and for their generous support of this research.

References

- Abercrombie, R. E., 1996, The magnitude-frequency distribution of earthquakes recorded with deep seismometers at Cajon Pass, southern California: *Tectonophysics*, v. 261, p. 1-7.
- Aki, K., 1987, Magnitude-Frequency Relation for Small Earthquakes: A Clue to the Origin of f_{max} of Large Earthquakes: *Journal of Geophysical Research*, v. 92, p. 1349-1355.
- Baig, A., and T. Urbancic, 2010, Microseismic moment tensors: A path to understanding frac growth: *The Leading Edge*, v. 29, p. 320-324.
- Boettcher, M. S., A. McGarr, and M. Johnston, 2009, Extension of Gutenberg-Richter distribution to $M < -1.3$, no lower limit in sight: *Geophysical Research Letters*, v. 36.
- East, L. E., W. Grieser, B. W. McDaniel, B. Johnson, R. Jackson, and K. Fisher, 2004, Successful Application of Hydrajet Fracturing on Horizontal Wells Completed in a Thick Shale Reservoir: *SPE Eastern Regional Meeting*.
- Eisner, L., S. Williams-Stroud, A. Hill, P. Duncan, and M. Thornton, 2010, Beyond the dots in the box: Microseismicity-constrained fracture models for reservoir simulation: *The Leading Edge*, v. 29, p. 326-333
- Fisher, M. K., J. R. Heinze, C. D. Harris, B. M. Davidson, C. A. Wright, and K. P. Dunn, 2004, Optimizing Horizontal Completion Techniques in the Barnett Shale Using Microseismic Fracture Mapping: *SPE Annual Technical Conference and Exhibition*, SPE-90051-MS.
- Gutenberg, B., and C. F. Richter, 1944, Frequency of earthquakes in California: *Bulletin of the Seismological Society of America*, v. 34, p. 185-188.
- Hanks, T. C., and H. Kanamori, 1979, A moment magnitude scale: *Journal of Geophysical Research*, v. 84, p. 2348-2350.
- Kidney, R. L., U. Zimmer, and N. Boroumand, 2010, Impact of distance-dependent location dispersion error on interpretation of microseismic event distributions: *The Leading Edge*, v. 29, p. 284-289.
- Maxwell, S. C., 2009, Assessing the Impact of Microseismic Location Uncertainties On Interpreted Hydraulic Fracture Geometries: *SPE Annual Technical Conference and Exhibition*, SPE-125121-MS.

- Maxwell, S. C., C. Waltman, N. R. Warpinski, M. J. Mayerhofer, and N. Boroumand, 2006, Imaging Seismic Deformation Induced by Hydraulic Fracture Complexity: SPE Annual Technical Conference and Exhibition, SPE-102801-MS.
- Maxwell, S. C., J. E. Shemeta, E. Campbell, and D. J. Quirk, 2008, Microseismic Deformation Rate Monitoring: SPE Annual Technical Conference and Exhibition, SPE-116596-MS.
- Mayerhofer, M. J., E. Lolon, N. R. Warpinski, C. L. Cipolla, D. W. Walser, and C. M. Rightmire, 2010, What Is Stimulated Reservoir Volume?: SPE Production & Operations, v. 25, p. pp. 89-98. SPE-119890-PA.
- Oye, V., H. Bungum, and M. Roth, 2005, Source Parameters and Scaling Relations for Mining-Related Seismicity within the Pyhasalmi Ore Mine, Finland: Bulletin of the Seismological Society of America, v. 95, p. 1011-1026.
- Shemeta, J., and P. Anderson, 2010, It's a matter of size: Magnitude and moment estimates for microseismic data: The Leading Edge, v. 29, p. 296-302.
- Sneddon, I. N., 1946, The Distribution of Stress in the Neighbourhood of a Crack in an Elastic Solid: Proceedings of the Royal Society of London. Series A. Mathematical and Physical Sciences, v. 187, p. 229-260.
- Soliman, M. Y., L. East, and D. Adams, 2008, Geomechanics Aspects of Multiple Fracturing of Horizontal and Vertical Wells: SPE Drilling & Completion, v. 23, p. pp. 217-228. SPE 86992-PA.
- Sprenke, K. F., M. C. Stickney, D. A. Dodge, and W. R. Hammond, 1991, Seismicity and tectonic stress in the Coeur d'Alene mining district: Bulletin of the Seismological Society of America, v. 81, p. 1145-1156.
- Trifu, C., Ioan, T. I. Urbancic, and R. P. Young, 1993, Non-similar frequency-magnitude distribution for $M < 1$ seismicity: Geophysical Research Letters, v. 20, p. 427-430.
- Urbancic, T. I., and S. C. Maxwell, 2002, Source Parameters of Hydraulic Fracture Induced Microseismicity: SPE Annual Technical Conference and Exhibition, SPE-77439-MS.
- Urbancic, T. I., V. Shumila, J. T. Rutledge, and R. J. Zinno, 1999, Determining hydraulic fracture behavior using microseismicity: Vail Rocks 1999, The 37th U.S. Symposium on Rock Mechanics (USRMS), 99-0991.
- von Seggern, D. H., J. N. Brune, K. D. Smith, and A. Aburto, 2003, Linearity of the Earthquake Recurrence Curve to $M < -1$ from Little Skull Mountain Aftershocks in Southern Nevada: Bulletin of the Seismological Society of America, v. 93, p. 2493-2501.
- Warpinski, N. R., and P. T. Branagan, 1989, Altered-Stress Fracturing: SPE Journal of Petroleum Technology, v. 41, p. 990-997. SPE-17533-PA.
- Warpinski, N., 2009, Microseismic Monitoring: Inside and Out: SPE Journal of Petroleum Technology, v. 61, p. 80-85. SPE-118537-MS.
- Waters, G. A., B. K. Dean, R. C. Downie, K. J. Kerrihard, L. Austbo, and B. McPherson, 2009, Simultaneous Hydraulic Fracturing of Adjacent Horizontal Wells in the Woodford Shale: SPE Hydraulic Fracturing Technology Conference, SPE-119635-MS.
- Williams-Stroud, S., 2008, Using Microseismic Events to Constrain Fracture Network Models and Implications for Generating Fracture Flow Properties for Reservoir Simulation: SPE Shale Gas Production Conference, SPE-119895-MS.
- Zoback, M. D., C. A. Barton, M. Brudy, D. A. Castillo, T. Finkbeiner, B. R. Grollmund, D. B. Moos, P. Peska, C. D. Ward, and D. J. Wiprut, 2003, Determination of stress orientation and magnitude in deep wells: International Journal of Rock Mechanics and Mining Sciences, v. 40, p. 1049-1076.